Global Environmental Change Advances 3 (2024) 100011

Contents lists available at ScienceDirect

Global Environmental Change Advances

journal homepage: www.sciencedirect.com/journal/global-environmental-change-advances

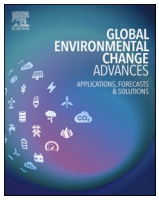

# Projected global sulfur deposition with climate intervention

H.J. Rubin [a,*], C.-E. Yang [a], F.M. Hoffman [b,a], J.S. Fu [a,b]

[a] Department of Civil and Environmental Engineering, University of Tennessee, Knoxville, TN, USA
[b] Computational Sciences and Engineering Division, Oak Ridge National Laboratory, Oak Ridge, TN 37831, USA

ARTICLE INFO

*Keywords:*
Sulfur deposition
SAI
Geoengineering
Climate intervention
Ecoregions

ABSTRACT

Even with immediate implementation of global policies to mitigate carbon dioxide emissions, the impacts of climate change will continue to worsen over the next decades. One potential response is stratospheric aerosol injection (SAI), where sulfur dioxide is released into the stratosphere to block incoming solar radiation. SAI does not reduce the level of carbon dioxide in the atmosphere, but it can slow warming and act as a stopgap measure to give the world more time to pursue effective carbon reduction strategies. While SAI is controversial, it remains a technically feasible proposition. It ought to be thoroughly modeled both to characterize global risks better and to further the scientific community's understanding of stratospheric aerosol dynamics. SAI relies on sulfate aerosols which have a lifetime of several years in the stratosphere but will eventually be deposited back onto Earth's surface. While sulfate is an important nutrient for many ecosystems, high concentrations can cause acidification, eutrophication, and biodiversity loss. We use model outputs from the Geoengineering Model Intercomparison Project (GeoMIP) to track the impacts of sulfur deposition from SAI to various ecoregions through comparison with historical climate and future Shared Socioeconomic Pathway (SSP) scenarios. Our results demonstrate that dry sulfur deposition will continue to decline worldwide, regardless of scenario, from a high of 41 Tg S/yr in 1981 to under 20 Tg S/yr by 2100. Wet sulfur deposition, however, is much more uncertain and further work needs to be done in this area to harmonize model estimates. Under SAI, many ecoregions will experience notably different sulfur deposition regimes by the end of the century compared to historical trends. In some places, this will not be substantially different than the impacts of climate change under SSP2–4.5 or SSP5–8.5. However, in some ecoregions the model projections disagree dramatically on the magnitude of future trends in both emissions and deposition, with, for example, UKESM1–0-LL projecting that $SO_4^{2-}$ deposition in deciduous needleleaf forests under G6 Sulfur will reach 394 % of SSP2–4.5 deposition by the 2080 s while CESM2-WACCM projects that $SO_4^{2-}$ deposition will remain at 170 % of SSP2–4.5 deposition during that same time period. Our work emphasizes the lack of agreement between models and the importance of improving our understanding of SAI impacts for future climate decision-making.

## 1. Introduction

Anthropogenic climate change is the most pressing global challenge we face today and the widespread harmful impacts to humans and ecosystems are being felt worldwide (Scheffers et al., 2016; IPCC, 2022). While scientists have warned for decades that it is essential to decrease carbon dioxide ($CO_2$) inputs to the atmosphere to mitigate climate change (d'Arge et al., 1982; Schultz and Kasting, 1997), current pledges to reduce emissions are not adequate to even maintain warming at two degrees Celsius above historical temperatures (Robiou du Pont and Meinshausen, 2018; Tollefson, 2019). A variety of responses will therefore be needed to slow warming, in addition to reducing emissions and adapting to the future warmer climate. This may include climate intervention (National Research Council, 2015). Climate intervention approaches fall into one of two categories: removing $CO_2$ from the atmosphere or modifying the way solar radiation is reflected by the atmosphere (Shepherd, 2012). While $CO_2$ removal will likely be part of a portfolio of responses to climate change, it may not be enough due to the costs of scaling $CO_2$ utilization (Hepburn et al., 2019). The most commonly researched method of altering the atmosphere's radiative budget is stratospheric aerosol injection (SAI) (Crutzen, 2006; Lawrence et al., 2018; Smith and Henly, 2021) using aircraft-based delivery (Tracy et al., 2022).

SAI is extremely controversial in part because it is a global

* Corresponding author.
*E-mail address:* hrubin@vols.utk.edu (H.J. Rubin).

https://doi.org/10.1016/j.gecadv.2024.100011
Received 23 February 2024; Accepted 25 July 2024
Available online 1 August 2024

intervention without clear policy frameworks or a governing body in charge of the decision to deploy, and in part because it calls into question both our duties and our rights towards the natural world and other humans. Studies disagree about the magnitude and impacts of disruptions to precipitation and temperature that it would cause (Clark et al., 2023; Irvine et al., 2019; Irvine and Keith, 2020; Kortetmäki and Oksanen, 2023). SAI is one of the only geoengineering options with the technological availability to feasibly deploy globally within a politically relevant timeframe (Grasso, 2019). SAI implementation costs are also relatively inexpensive compared to the cost of mitigating temperature warming to less than 1.5 degrees Celsius or the costs of unmitigated climate change (Smith and Wagner, 2018). Decreasing radiative forcing does not address the fundamental issue of the high concentration of greenhouse gases in the atmosphere, but it would allow more time for the world to reduce and stabilize emissions in the very near term. While it should not distract from the work of actually reducing emissions on a global scale or developing carbon removal technology, SAI remains a viable stopgap measure and ought to be investigated thoroughly from a modeling perspective (Long and Shepherd, 2014; Xu et al., 2020).

There is a growing body of scientific research on global temperature and precipitation patterns that may be altered by SAI (Irvine et al., 2019; Irvine and Keith, 2020; Lee et al., 2020), similar to the way volcanic aerosols alter radiation (Gu et al., 2003), but other environmental variables are less well constrained. Sulfate deposition is of particular interest because sulfur dioxide ($SO_2$) injected into the stratosphere will quickly produce sulfate aerosols. Atmospheric sulfur deposition is an important part of many biogeochemical cycles (Pye et al., 2020; Tjiputra et al., 2016). However, when exceeding critical loads, sulfur can have harmful impacts on both human and ecosystem health. Anthropogenic sulfur deposition can also cause declines in the pH of both marine and non-marine waterbodies, slightly increasing ocean and freshwater acidification and harming fish populations (Doney et al., 2007; Neary and Dillon, 1988; Shao et al., 2020). SAI takes place in the stratosphere, not the troposphere, but there are interactions between the two and the aerosol particles will settle to the surface within a few years (Visioni et al., 2020).

One study comparing GEOS-Chem and ULAQ-CCM found that sulfur deposition will increase when sulfate geoengineering is deployed (Visioni et al., 2018). Currently, 125 Tg of $SO_2$ is emitted into the atmosphere annually from anthropogenic sources, although this is trending down (Aas et al., 2019). To maintain the global temperature at 1.5° C above the historical average with SAI, about 29 Tg of additional $SO_2$ would be required annually by the end of the century, although this amount depends on injection strategy and deployment (Niemeier and Timmreck, 2015; Visioni et al., 2021). The sulfur deposition would also be impacted by unmitigated climate change as increased greenhouse gases in the atmosphere react with the hydrological cycle (Tracy et al., 2022). It is important to determine where the sulfur deposition will end up and over what time frame both with and without SAI.

The Climate Model Intercomparison Project Phase 6 (CMIP6) is organized by the World Climate Research Program (WCRP)'s Working Group of Coupled Modeling (WGCM) to coordinate climate model experiments worldwide, using common protocols, climate forcing, and output formats to provide future climate projections (Eyring et al., 2016). The newest iterations of the CMIP models are based on a possible climate outcome from a Representative Concentration Pathway (RCP) between 1.9 and 8.5 W/m$^2$ of radiative forcing matched with a Shared Socioeconomic Pathway (SSP 1–5) (O'Neill et al., 2016). The SSPs describe the potential social development that might in the future occur based on factors like population size, education, energy demand, and other non-climate factors (Riahi et al., 2017). The Geoengineering Model Intercomparison Project (GeoMIP) is a suite of climate model experiment designs built on CMIP6 simulations to address geoengineering as a response to climate change (Kravitz et al., 2015, 2011). The G6sulfur scenario includes stratospheric sulfate aerosol injection to reduce net forcing from SSP5–8.5 to SSP2–4.5. SSP5 combined with RCP8.5 is often referred to as the "worst-case" climate scenario for our world, with 8.5 W/m$^2$ of radiative forcing and socioeconomic conditions characterized by a reliance on fossil fuels for development. SSP2–4.5 is a moderate case climate scenario with 4.5 W/m$^2$ radiative forcing and a middle-of-the-road approach without extreme social, economic, technological, or land use changes from historical patterns. We use the outputs of the three earth system models available from the CMIP6 archive for G6sulfur, SSP2–4.5, and SSP5–8.5 to investigate the long-term impacts of SAI on sulfur deposition.

## 2. Methods and Data

This study utilized the G6sulfur model outputs from the CMIP6 archive (available at https://esgf-node.llnl.gov/projects/cmip6) to analyze sulfur deposition changes due to SAI under climate change. Since G6sulfur is designed to reduce net radiative forcing from SSP5–8.5 to SSP2–4.5 (Visioni et al., 2021), we also retrieved model outputs from SSP5–8.5 and SSP2–4.5 for comparisons. Across the CMIP6 archive, only three models provide sulfur deposition-relevant variables—wet $SO_2$, dry $SO_2$, wet $SO_4^{2-}$, dry $SO_4^{2-}$, and precipitation flux—under the G6sulfur scenario (Table 1). Hence, we retrieved the outputs from these three models under SSP5–8.5 and SSP2–4.5 for fair comparisons. Historical outputs during 1950–2014 were also retrieved for the same models to compare with the three future scenarios. None of the models explicitly incorporate bi-directional flux for sulfur. All three models include interactive stratospheric chemistry but only UKESM1-0-LL and CESM2-WACCM include interactive aerosol microphysical schemes while CNRM-ESM2-1 uses prescribed ozone fields (Séférian et al., 2019; Tilmes et al., 2022). UKESM1-0-LL and CESM2-WACCM include interactive aerosol microphysical models and inject $SO_2$ at specific latitudes and CNRM-ESM2-1 uses an input dataset from the GeoMIP G4 Specified Stratospheric Aerosols (G4SSA) experiment to prescribe the aerosol distribution and optical properties such that the target temperature is reached (Tilmes et al., 2015). Despite this, we include CNRM-ESM2 deposition variables for comparison with the other two models.

The 13 ecoregions were defined by clustering climate, soil, and topography types and fitting the categories to the International Geosphere-Biosphere Programme (IGBP) ecoregion definitions (Hargrove et al., 2006; Hargrove and Hoffman, 2004; Townshend, 1992), following Yang et al. (2020). All analysis was done with R (R Core Team, 2022); available at https://www.r-project.org/) and Climate Data Operators (CDO, Schulzweida, 2021; available at https://code.mpimet.mpg.de/projects/cdo).

## 3. Results

Historically, sulfur deposition peaked on a global scale in the 1980s (Smith et al., 2004). This peak can be seen in all three ESMs in Figure S1, which shows historical dry deposition and future estimated dry deposition for each ESM in Table 1. Dry S is projected to decline consistently from a peak of $4.33 \times 10^{-12} \pm 1.39$ kg/m$^2$s through 2100–$1.71 \pm 0.51 \times 10^{-12}$ kg/m$^2$s for all three G6sulfur models and to $1.41 \pm 0.28 \times 10^{-12}$

**Table 1**
Summary of selected CMIP6 model outputs in this work.

| Earth System Models | Horizontal Grid Resolution | Climate Scenario | | | |
|---|---|---|---|---|---|
| | | Historical | SSP2-4.5 | SSP5-8.5 | G6sulfur |
| CESM2-WACCM | 192×288 | r1p1i1f1 | r1p1i1f1 | r1p1i1f1 | r1p1i1f2 |
| CNRM-ESM2–1 | 128×256 | r1p1i1f2 | r1p1i1f2 | r1p1i1f2 | r1p1i1f2 |
| UKESM1–0-LL | 144×192 | r1p1i1f2 | r1p1i1f2 | r1p1i1f2 | r1p1i1f2 |

kg/m$^2$s under SSP2–4.5 and 1.47±0.32 × $10^{-12}$ kg/m$^2$s under SSP5–8.5 projections (Fig. 1) because of declining anthropogenic emissions (Cheng et al., 2022; Zhou et al., 2021).

## 4. Model Discrepancies

Fig. 2 shows the wet deposition trends by model under G6sulfur. The three models agree well enough on dry deposition trends to ensemble them together into a multi-model mean (Fig. 1), but the models do not agree on wet deposition trends. UKEMS1–0-LL projects relatively consistent wet $SO_4^{2-}$, around × $10^{-12}$ kg/m$^2$s, lower than the historical peak of the 1980s (7.55±0.06 × $10^{-12}$ kg/m$^2$s). Wet $SO_2$ deposition is projected to consistently decrease from 1.23±0.17 × $10^{-12}$ kg/m$^2$s to 9.36±0.11 × $10^{-13}$ kg/m$^2$s by 2100 (Fig. 2A). However, under both SSP2–4.5 and SSP5–8.5, wet $SO_2$ is expected to decline from 1.36 ±0.14 × $10^{-12}$ to 8.91±0.01 × $10^{-13}$ kg/m$^2$s and 1.37±0.18 × $10^{-12}$ kg/m$^2$s to 8.71±0.12 × $10^{-13}$ kg/m$^2$s, respectively. Wet $SO_4^{2-}$, similarly, is expected to decline under the two SSP scenarios from 6.44 ±0.32 × $10^{-12}$ to 3.86±0.18 × $10^{-12}$ under SSP2–4.5 and from 3.73 ±0.34 × $10^{-12}$ kg/m$^2$s to 6.46±0.39 × $10^{-12}$ kg/m$^2$s under SSP5–8.5

In terms of seasonality, according to UKESM1–0-LL, both wet $SO_4^{2-}$ and wet $SO_2$ remain constant throughout the year under G6sulfur (an average of 5.57±0.02 × $10^{-12}$ kg/m$^2$s for wet $SO_4^{2-}$ and 1.09±0.01 × $10^{-12}$ kg/m$^2$s for wet $SO_2$), SSP2–4.5 (an average of 4.77±1.31 × $10^{-12}$ kg/m$^2$s for wet $SO_4^{2-}$ and 1.06±0.03 × $10^{-12}$ kg/m$^2$s for wet $SO_2$), and SSP5–8.5 (an average of 5.15±1.38 × $10^{-12}$ kg/m$^2$s for wet $SO_4^{2-}$ and 1.09±0.03 × $10^{-12}$ kg/m$^2$s for wet $SO_2$) throughout the year with a high in December/January and a low in the northern hemisphere summer season as precipitation increases from 3.12±0.08 mm/day to 3.25 ±0.06 mm/day. This is not consistent with historical patterns of wet $SO_2$ deposition which has historically declined during May-October, or with historical patterns of wet $SO_4^{2-}$ deposition which has, on average, increased during these months (Fig. 2B).

CESM2-WACCM projects a slight increase in precipitation from 2.89 ±1.04 mm/day in 1950–3.03±0.08 mm/day through 2075 (Figure S2) and a large increase in wet $SO_4^{2-}$ deposition, with deposition dipping down below 1960s levels (5.63±0.55 × $10^{-12}$ kg/m$^2$s) until the 2050 s and then increasing steadily to nearly as high as the 1980s peak (6.59 ±0.78 × $10^{-12}$ kg/m$^2$s) by the end of the century (Fig. 2B). Wet $SO_2$ deposition is projected to decrease from 1.49±0.18 × $10^{-12}$ kg/m$^2$s in 2020–8.58±0.95 × $10^{-13}$ kg/m$^2$s by 2100. Under SSP2–4.5 wet $SO_4^{2-}$ is projected to decline consistently from the 1980s peak to 3.97±0.04 × $10^{-12}$ by 2100 and wet $SO_2$ is projected to decline to 8.36±1.22 × $10^{-13}$ over the same time period.

On a seasonal basis, historically wet $SO_4^{2-}$ has increased slightly during May-October as precipitation increases. However, under G6 Sulfur, the CESM2-WACCM model projects a slight decline during those months from 6.67±0.84 × $10^{-12}$ kg/m$^2$s to 5.75±0.62 × $10^{-12}$ kg/m$^2$s for $SO_4^{2-}$ and a slight increase from 1.08±0.34 × $10^{-12}$ kg/m$^2$s to 1.33 ±0.47 × $10^{-12}$ kg/m$^2$s for wet $SO_2$, as precipitation increases to 3.09 ±.10 mm/day from 2.89±0.07 mm/day. Under SSP2–4.5 and SSP5–8.5 wet $SO_4^{2-}$ is projected to remain constant at 5.07±1.42 × $10^{-12}$ kg/m$^2$s and 5.33± 1.49× $10^{-12}$ kg/m$^2$s respectively. Precipitation increases during the northern hemisphere summer months from a low of 2.94 ±0.00 mm/day to 3.13±0.00 mm/day under SSP2–4.5 and 2.80 ±0.01 mm/day to 3.16±0.01 mm/day under SSP5–8.5.

According to the CNRM-ESM2–1 model, precipitation has historically remained constant at 2.94±0.00 mm/day from the 1950s to the present day. Under G6 Sulfur, this trend is projected to continue at 2.99 ±0.00 mm/day. However, under SSP2–4.5, precipitation is projected to increase to 3.09±0.00 mm/day and under SSP5–8.5, it will increase to 3.18±0.00 mm/day by 2100. All 3 scenarios project a large decline in wet $SO_4^{2-}$ deposition from the 1980s peak of 8.49±0.88 × $10^{-12}$ kg/m$^2$s to 3.45±0.75 × $10^{-12}$ kg/m$^2$s for G6 Sulfur, for SSP2–4.5, and for SSP5–8.5 by 2100 (Fig. 2B). Unlike the other two ESMs, CNRM-ESM2–1 historical estimates show that wet $SO_4^{2-}$ has decreased during May-October from 8.42±0.05 × $10^{-12}$ kg/m$^2$s to 6.58±0.01 × $10^{-12}$ kg/m$^2$s. This pattern is consistent with G6 Sulfur projections which estimate a low of 4.26±0.05 × $10^{-12}$ kg/m$^2$s and a high of 5.75±0.05 × $10^{-12}$ kg/m$^2$s. Under SSP2–4.5 and SSP5–8.5 wet $SO_4^{2-}$ deposition is relatively constant at 4.84±1.72 × $10^{-12}$ kg/m$^2$s and 5.01±21.81 × $10^{-12}$ kg/m$^2$s, respectively. Precipitation increases during May-October under G6 Sulfur, SSP2–4.5, and SSP5–8.5 from a low of 2.93 mm/day to a high of 3.06 mm/day and a low of 2.97 mm/day to a high of 3.09 mm/day and a low of 2.99 mm/day to a high of 3.11 mm/day, respectively. CNRM-ESM2–1 projections do not include publicly available wet $SO_2$.

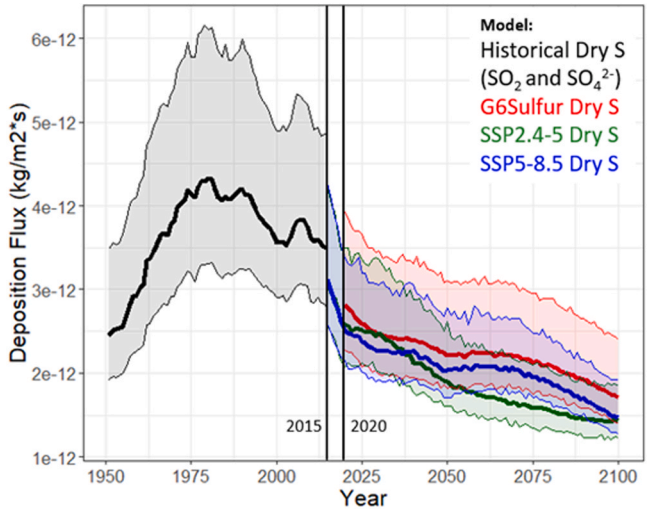


**Fig. 1.** Global dry S (both $SO_2$ and $SO_4^{2-}$) deposition flux from historical estimates and three future climate scenario projections, SSP2–4.5, SSP5–8.5, and G6sulfur. The solid lines represent the ensemble mean and the shaded region is the spread across models. The differences between models can be seen in Fig. S1.

## 5. SAI by Ecoregions

Focusing on CESM2-WACCM and UKESM1–0-LL projections (the two models with publicly available projections for both $SO_2$ and $SO_4^{2-}$ deposition) by ecoregion highlights the parts of the world most likely to be impacted by excess sulfur deposition under G6Sulfur compared to climate change under SSP2–4.5 (Fig. 3). The comparison between G6 Sulfur and SSP5–8.5 is shown in Figure S4.

According to the CESM2-WACCM model, $SO_2$ emissions under G6 Sulfur will be higher in 2020–2040 compared to SSP2–4.5 emissions and decline with each progressive decade in savannas, grasslands, and barren or sparsely vegetated lands (Fig. 3). In non-marine water bodies, deciduous needleleaf forests, mixed forests, open shrublands, woody savannas, croplands/natural vegetation mosaics, and permanent snow and ice, results are more mixed, with higher emissions under G6 Sulfur in the mid-century only to decline back to or below the SSP2–4.5 emission rate by 2100. And in evergreen needleleaf forests, evergreen broadleaf forests, and croplands $SO_2$ emissions experience negligible change from SSP2–4.5 levels.

According to the CESM2-WACCM model, $SO_4^{2-}$ emissions are projected to be higher from 2020 to 2040 under G6 Sulfur than SSP2–4.5 and decline with each progressive decade through 2100 in non-marine

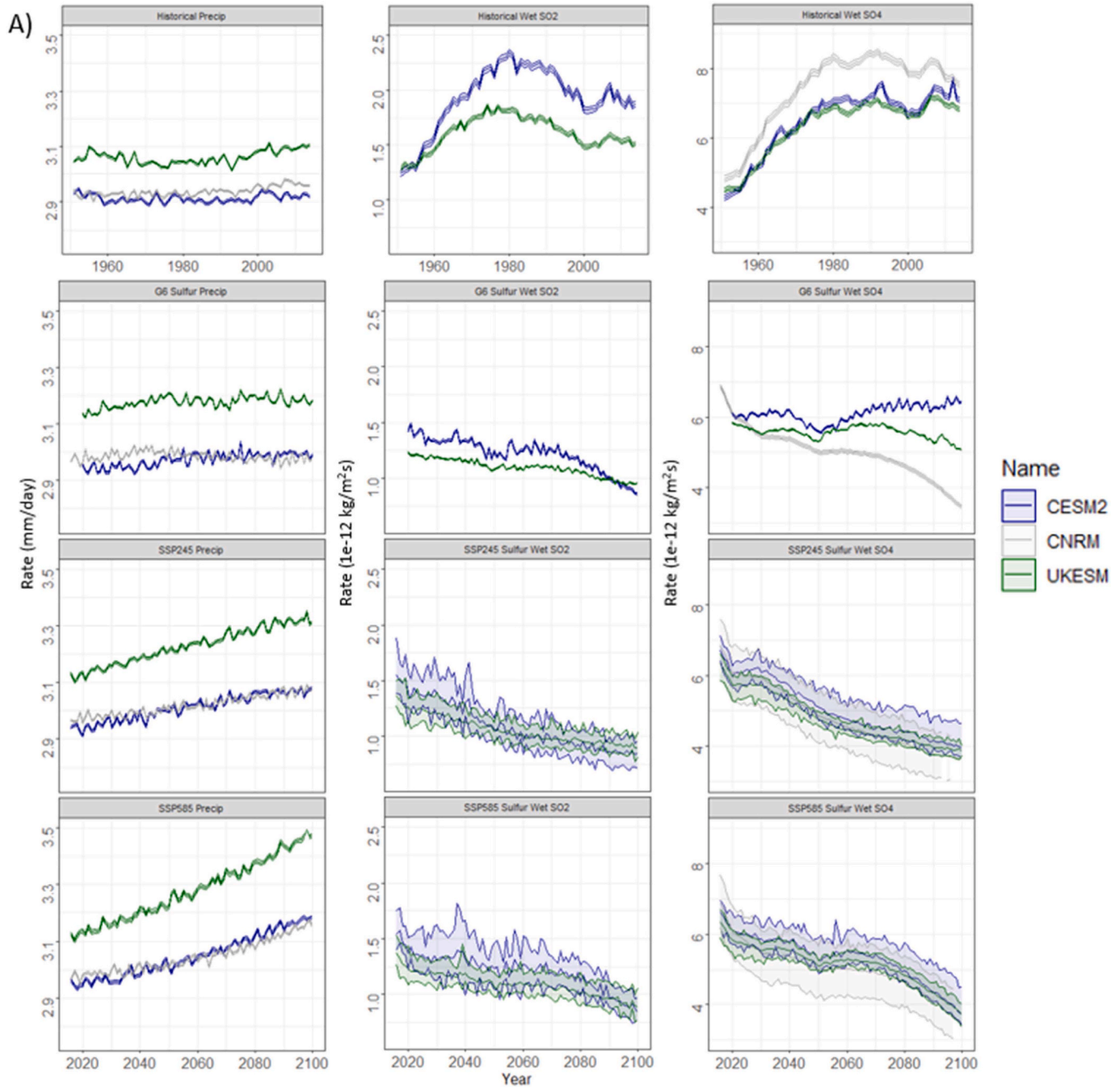


**Fig. 2.** Projected **A)** annual and **B)** monthly precipitation and wet sulfur ($SO_2$ and $SO_4^{2-}$) deposition from UKESM1–0-LL, CESM2-WACCM, and CNRM-ESM2–1 during the historical time period (1980–2020) and under G6 Sulfur, SSP2–4.5, and SSP5–8.5 conditions (2020–2100).

water bodies (from 267 % to 98 %), evergreen broadleaf forests (123–93 %), mixed forests (from 170 % to 113 %), savannas (from 180 % to 38 %), grasslands (from 143 % to 76 %), croplands (from 134 % to 82 %), and barren or sparsely vegetated lands (from 136 % to 51 %). In deciduous needleleaf forests and open shrublands, $SO_4^{2-}$ emissions increase mid-century relative to SSP2–4.5 (184 % and 166 %, respectively) only to decline to less than 100 % by 2081–2100. In woody savannas, emissions are consistently higher than SSP2–4.5 emissions. In evergreen needleleaf forests emissions remain constant at 100 % of SSP2–4.5 levels. And in croplands/natural vegetation mosaics and permanent snow and ice $SO_4^{2-}$ emissions drop below 100 % of the SSP2–4.5 rate mid-century only to increase to 140 % and 107 %, respectively, of SSP2–4.5 levels by 2081–2100.

Under G6 Sulfur, $SO_2$ deposition according to the CESM2-WACCM model declines relative to SSP2–4.5 levels from close to 150 % to less than 100 % in non-marine water bodies (from 147 % to 97 %), deciduous needleleaf forests (from 199 % to 110 %), mixed forests (from 150 % to 83 %), savannas (from 175 % to 49 %), permanent snow and ice (from 162 % to 42 %), and barren or sparsely vegetated lands (from 153 % to 47 %). In open shrublands and croplands/natural vegetation mosaics, there is no difference between G6 Sulfur and SSP2–4.5 $SO_2$ deposition throughout the century. Two ecoregions experience a decrease during 2041–2060 compared to SSP2–4.5 levels – from 133 % to 101 % in evergreen needleleaf forests and from 116 % to 91 % in grasslands. Other ecoregions instead will experience greater $SO_2$ deposition relative to SPSP2–4.5 during this time period: evergreen broadleaf

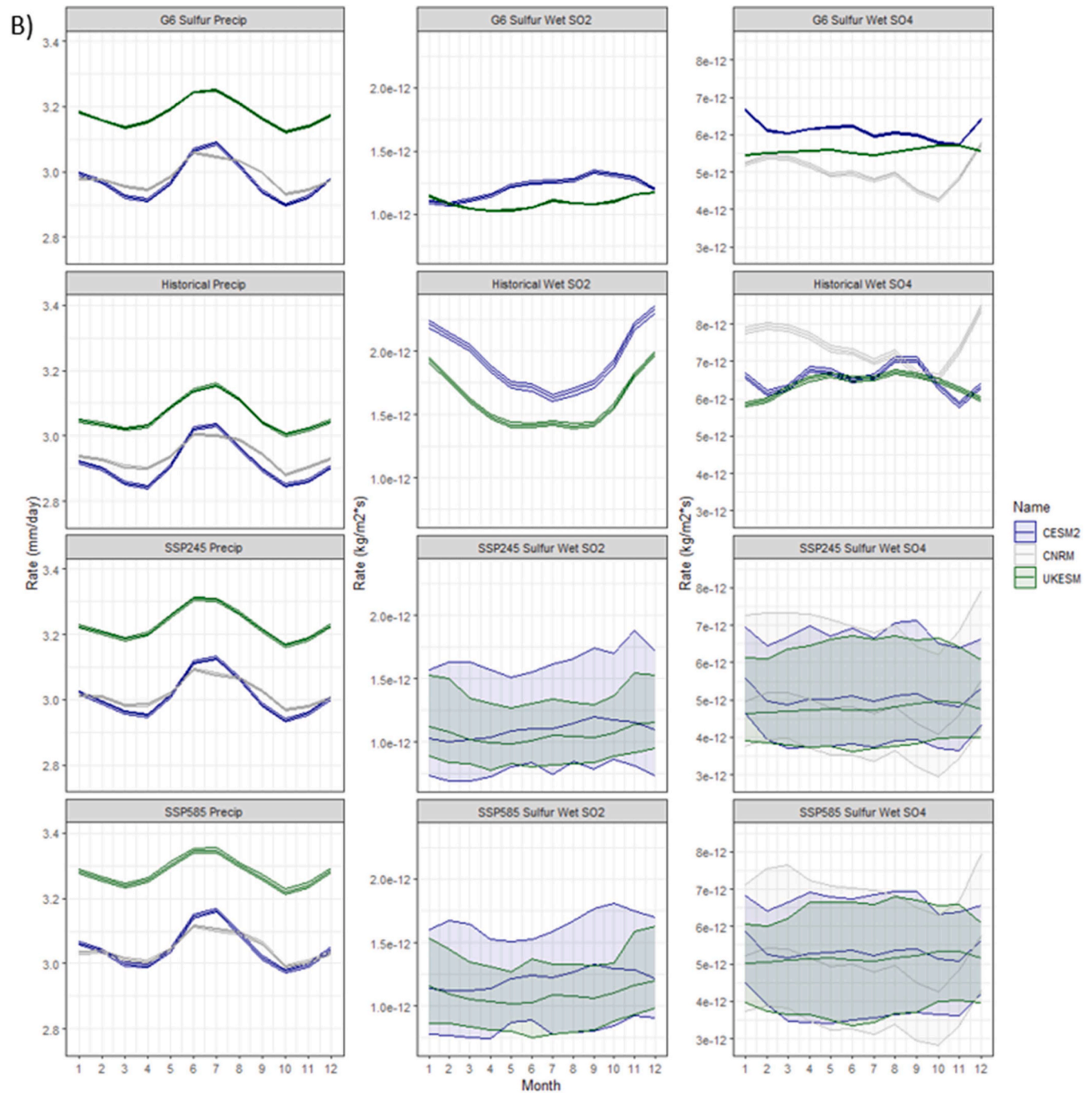


**Fig. 2.** (*continued*).

forests (from 130 % to 170 %), woody savannas (from 140 % to 190 %), and croplands (from 106 % to 163 %).

According to the CESM2-WACCM model, $SO_4^{2-}$ deposition is projected to be higher under G6 Sulfur than SSP2–4.5 in the 2020 s and decline relative to SSP2–4.5 by 2100 in woody savannas (from 163 % to 120 %), savannas (from 224 % to 86 %), permanent snow and ice (from 179 % to 90 %), and barren or sparsely vegetated lands (from 149 % to 87 %). $SO_4^{2-}$ emissions are projected to increase by the end of the century in non-marine water bodies (from 95 % to 138 %), deciduous needleleaf forests (from 99 % to 170 %), mixed forests (from 118 % to 128 %), and open shrublands (from 94 % to 130 %) relative to SSP2–4.5. $SO_4^{2-}$ emissions will decline through 2061–2080 and then increase again relative to SSP2–4.5 in evergreen needleleaf forests (from 122 % to 143 %), grasslands (from 89 % to 112 %) and croplands (from 95 % to 110 %). In evergreen broadleaf forests, $SO_4^{2-}$ deposition is greater relative to SSP2–4.5 levels through 2061–2080–144 % of SSP2–4.5 deposition and then declines to 99 %. In croplands/natural vegetation mosaics, $SO_4^{2-}$ deposition declines to 86 % of SSP2–4.5 deposition in 2041–2060 and then increases to 171 % by 2080–2100.

According to the UKESM1–0-LL projections, $SO_2$ emissions will increase relative to SSP2–4.5 in woody savannas from 124 % to 369 % by 2081–2100. $SO_2$ emissions are projected to decline relative to SSP2–4.5 in non-marine water bodies (from 142 % to 92 %), evergreen broadleaf forests (from 146 % to 84 %), deciduous needleleaf forests (from 124 % to 64 %), mixed forests (from 128 % to 100 %), open shrublands (from 116 % to 73 %), savannas (from 200 % to 46 %), grasslands (from 230 % to 62 %), and barren or sparsely vegetated lands (from 200 % to 57 %) throughout the century (Fig. 3). Emissions are projected to remain

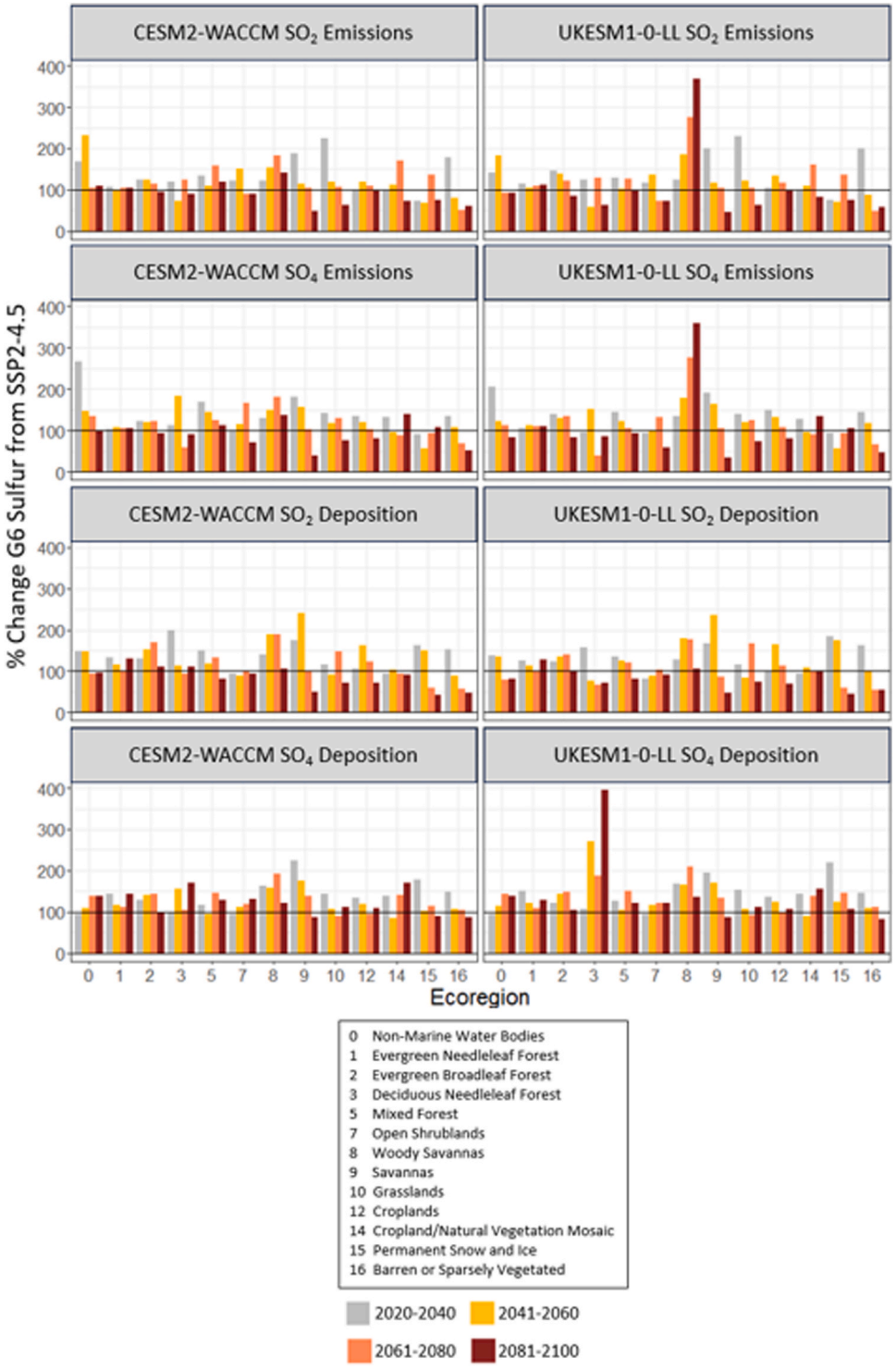


**Fig. 3.** The percent change from SSP2–4.5 to G6Sulfur for CESM2-WACCM and UKESM1–0-LL $SO_2$ and $SO_4^{2-}$ deposition by ecoregion, calculated as a difference in total deposition in Tg-S/yr. and the percent change from SSP5–8.5 is shown in Fig. S4.

constant at 110 % of the SSP2–4.5 rate in evergreen needleleaf forests while emissions in croplands, cropland/natural vegetation mosaics and permanent snow and ice are projected to increase under G6 Sulfur to 133 %, 160 %, and 137 % respectively, relative to SSP2–4.5 during 2041–2060 and 2061–2080 then decline back to just under 100 % of SSP2–4.5 levels.

According to the UKESM1–0-LL projections, $SO_4^{2-}$ emissions under G6 Sulfur will decline relative to SSP2–4.5 emissions in non-marine water bodies (from 206 % to 84 %), evergreen broadleaf forests (from 140 % to 83 %), mixed forests (from 145 % to 92 %), savannas (from 192 % to 35 %), grasslands (from 139 % to 74 %), croplands (from 148 % to 80 %), and barren or sparsely vegetated lands (from 145 % to 45 %) by the end of the century. $SO_4^{2-}$ emissions are projected to increase relative to SSP2–4.5 in woody savannas from 134 % in 2020–2040–359 % in 2081–2100. $SO_4^{2-}$ emissions in evergreen needleleaf forests are projected to remain constant at 105 % of the SSP2–4.5 rate but emissions in deciduous needleleaf forests will increase to 152 % of the SSP2–4.5 rate in 2041–2060 then decrease to 38 % in 2061–2080 then increase again to

86 % by 2081–2100. Open shrublands will experience an increase to 133 % of SSp2–4.5 levels in 2061–2080 then a decline to 59 % in the next 2 decades. $SO_4^{2-}$ emissions in cropland/natural vegetation mosaics and permanent snow and ice decline mid-century to 96 % and 57 % of SSP2–4.5 levels, respectively, then increase to 135 % and 106 % by the end of the century.

Under G6 Sulfur, $SO_2$ deposition will decline in non-marine water bodies (from 138 % to 80 %), evergreen broadleaf forests (from 126 % to 99 %), 3 (from 158 % to 71 %), mixed forests (from 137 % to 81 %), open shrublands (from 80 % to 91 %), permanent snow and ice (from 184 % to 45 %), and barren or sparsely vegetated lands (from 162 % to 54 %) by the end of the century when compared to SSP2–4.5 $SO_4^{2-}$ deposition. $SO_2$ deposition is projected to increase relative to SSP2–4.5 by mid-century in woody savannas (from 128 % to 180 %), savannas (from 168 % to 236 %), grasslands (from 115 % to 167 %), croplands (from 102 % to 164 %) and then decline below the original percentage. And $SO_2$ deposition is constant under G6 Sulfur at 100 % of rate SSP2–4.5 rate in cropland/natural vegetation mosaics and constant at 126 % of the SSP2–4.5 rate in evergreen needleleaf forests.

$SO_4^{2-}$ deposition will increase under G6 Sulfur according to the UKESM1–0-LL projections in non-marine water bodies (from 94 % to 139 %), deciduous needleleaf forests (from 106 % to 394 %), open shrublands (from 94 % to 122 %), and cropland/natural vegetation mosaics (from 145 % to 156 %) relative to SSP2–4.5 estimates. It will decrease in savannas (from 196 % to 88 %), grasslands (from 152 % to 112 %), croplands (from 136 % to 107 %), permanent snow and ice (from 220 % to 107 %), and barren or sparsely vegetated lands (from 146 % to 82 %) relative to SSP2–4.5 deposition rates. Under G6 Sulfur, $SO_4^{2-}$ deposition in evergreen broadleaf forests increases mid-century from 122 % to 148 % and evergreen needleleaf forests decreases from 151 % to 108 % mid-century then returns to 129 % of SSP2–4.5 deposition by 2081–2100. Deposition in mixed forests and woody savannas decreases mid-century to 105 % and 166 % relative to SSP2–4.5 levels, respectively, then increases to 151 % and 210 %, respectively, by the end of the century.

## 6. Discussion

Past projections from CESM1-WACCM estimate a total global deposition rate of 40 Tg-S $yr^{-1}$ in 2020, declining to 23 Tg-S $yr^{-1}$ by 2100 under RCP8.5 (Visioni et al., 2020). However, in this study, CESM2-WACCM projects a total global deposition rate of 71.6 Tg-S $yr^{-1}$ in 2020, increasing to 82.0 Tg-S $yr^{-1}$ by 2100 under SSP5–8.5 and UKESM-1–0-LL projects a total global deposition rate of 65.1 Tg-S $yr^{-1}$ in 2020, increasing to 74.5 Tg-S $yr^{-1}$ by 2100 under SSP5–8.5. These values are more similar to historical estimates. Two other models estimate total S deposition as 76.8 Tg-S $yr^{-1}$ and 93.3 Tg-S $yr^{-1}$ on average for 2000–2005 GEOS-Chem and University of L'Aquila Composition-Chemistry Model (ULAQ-CCM), respectively (Visioni et al., 2018). Total global sulfur deposition in 2010 was estimated at 88.8 Tg-S (Rubin et al., 2023). Total global sulfur emissions in 2015 were around 120 Tg-S (Aas et al., 2019) with deposition presumably slightly lower (Lamarque et al., 2013; Visioni et al., 2017).

Dry $SO_4^{2-}$ and dry $SO_2$ deposition will continue to decline globally under G6sulfur, SSP2–4.5, and SSP5–8.5, dropping sharply throughout the 2030 s and 2040 s and plateauing below 1950s levels by 2100 (Fig. 1). The consistency of projections between scenarios and models demonstrates that injecting sulfate into the stratosphere does not fundamentally change the mechanisms influencing dry deposition on a global scale. Similarly, increasing the radiative forcing by increasing the $CO_2$ in the atmosphere compared to present day conditions (as under SSP5–8.5 or SSP2–4.5) does not influence the atmospheric chemistry and material properties of the dry sulfur particles settling out of the atmosphere.

Prior research shows that decreasing radiative forcing will decrease precipitation rates in many regions, therefore decreasing the rainout of particulate matter and resulting in longer lifetimes and more exposure to particulate matter remaining in the atmosphere under lower radiative forcing scenarios (Eastham et al., 2018). Precipitation is predicted to increase under all three scenarios (Figure S2) when compared to historical conditions, although under G6Sulfur precipitation will begin to decline again by 2050. Precipitation tends to remove $PM_{2.5}$ from the atmosphere so it follows that as the frequency of rainy days decreases in some places, even as the intensity increases, dry deposition will become the more dominant process. This means that the ratio of wet to dry deposition will steadily decline as precipitation increases. Wet deposition is more efficient at removing smaller aerosols so as rates of wet deposition decline, these smaller aerosols will tend to remain in the atmosphere longer.

Although the three ESMs disagree on the magnitude and trend in wet $SO_4^{2-}$ under G6sulfur (Fig. 2), they do agree that wet $SO_2$ will continue its current decline. Similarly, all three ESMs project a fundamental shift in seasonal $SO_4^{2-}$ deposition where, even as precipitation increases from May to October, deposition decreases. This trend would make sense for dry deposition; as precipitation increases, more particles are rained out and so there is less dry deposition. But for more wet deposition to occur even as precipitation decreases shows that there is a process – in this case SAI – continually adding $SO_4^{2-}$ to the system.

The three models have different features included in the simulated stratosphere and aerosol transport and deposition. The deposition patterns by latitude (Figure S3) demonstrate that the amount of $SO_2$ remaining in the stratosphere varies by injection scheme. All three models have a peak in deposition at 0°, 45°, and −45°, but the magnitudes vary by model and by time period, with different latitudes experiencing either steady increasing or decreasing deposition throughout the century. This is likely because a) the amount of $SO_2$ needed to reach the AOD necessary to cool the planet varies between models due to different $SO_2$ to sulfate conversion rates (Visioni et al., 2023) by as much as 10 Tg/year, and b) even though $SO_2$ is supposed to remain in the stratosphere as long as possible, it will inevitably eventually precipitate. Additionally, the injection altitude will impact stratospheric heating and result in temperature and precipitation differences between models. A large part of the uncertainty in $SO_4^{2-}$ is due to differences in the aerosol chemistry in each model, specifically the $SO_2$ to $SO_4^{2-}$ conversion rate (Visioni et al., 2023).

This is because of the way solar reduction is treated in the three ESMs. All ESMs reach SSP2–4.5 by the end of the century, but their approaches differ (Tilmes et al., 2022). They begin in 2020 with SSP5–8.5 emissions and then a sulfate aerosol optical depth (AOD) is added to reflect sunlight and cool the planet to reach SSP2–4.5 levels of radiative forcing. UKESM1–0-LL injects $SO_2$ uniformly between 10° N and 10° S between 18 and 20 km of altitude and across a single longitudinal band (0°). CESM2-WACCM injects $SO_2$ at the equator at an altitude of 25 km. CNRM-ESM2–1 uses an input dataset from a different GeoMIP experiment (G4SSA) to prescribe the aerosol optical depth distribution. The UKESM-1 model adjusts the AOD every decade whereas CESM2-WACCM and CNRM-ESM2 adjust every year.

Our analysis of emissions and deposition by ecoregion demonstrates that the type and location of ecoregion will determine whether it receives more sulfur deposition under G6 Sulfur compared to climate change under either SSP2–4.5 or SSP5–8 (Fig. 3). Visioni et al. (2020) write that according to CESM1-WACCM projections, more deposition will occur in pristine areas under G6 Sulfur compared to the historical period as long-range transport relocates the particles away from the site of emissions to mid- and high- latitudes. This poses a risk to ecoregions that are particularly sensitive to fluctuations in sulfur levels and may not be able to survive rapid changes. Critical loads are the threshold of atmospheric deposition below which ecological harm does not occur for any given ecosystem or species (Nilsson, 1988). Beyond the critical load for an ecosystem, acidification and eutrophication will occur and important biogeochemical cycles will be impacted (Driscoll et al., 2001; Galloway, 1995; Lanning et al., 2019). In US forests, the critical load for

sulfur deposition can be calculated for lichen and used as an indicator of overall forest health, because lichen is particularly sensitive to air pollution (Geiser et al., 2021; McMurray et al., 2021). One study calculates this value to be 2.7 kg S $ha^{-1}$ $y^{-1}$ for forested ecosystems in the US (Geiser et al., 2021), or 8.56 × $10^{-11}$ kg S/$m^2$s. By this measure, the only ecoregion annual averages below the critical load under both G6Sulfur and SSP2–4.5 are deciduous needleleaf forests for 2020–2100 and Croplands/Natural Vegetation Mosaic for 2061–2100. Under SSP5–8.5, the ecoregions below the critical load are deciduous needleleaf forests for 2020–2100 and Croplands/Natural Vegetation Mosaic for 2081–2100. While not all species are not as sensitive to sulfur deposition as lichens, and there is a large range in both critical loads and uncertainty in critical loads by species, forest type, and underlying soil (Ge et al., 2023; Pavlovic et al., 2023), the exceedance in so much of the world is concerning.

It is also important not to compare a climate intervention scenario to the current climate but rather to other possible futures to understand the risks of different global actions. When compared to SSP2–4.5, G6sulfur $SO_4^{2-}$ deposition does not decrease as quickly and in some ecoregions begins to rise again by the end of the 21st century. Emissions, on the other hand, are lower and drop faster. When compared to SSP5–8.5, emissions and deposition tend to be lower across the board, although, again, in several ecoregions, $SO_4^{2-}$ deposition will be higher by the end of the century. These results suggest that for most of the world, both SSP2–4.5 and SSP5–8.5 are associated with lower deposition by the end of the century. Nevertheless, in the near future, the opposite is true, meaning that benefits (strictly defined as lower sulfur deposition to sensitive ecosystems) from SAI will be concentrated in the next 20 years. One important note with our analysis is that these ecoregions will likely not be located in the same locations by the end of the century due to climate change and land use change (Wu et al., 2015).

$SO_2$ emissions are higher than deposition under all three scenarios (Fig. 3) but $SO_4^{2-}$ deposition is higher than $SO_4^{2-}$ emissions due to the atmospheric chemistry taking place as $SO_2$ is transformed into sulfate. Under SSP2–4.5 and SSP5–8.5 sulfate deposition decreases over time as $SO_2$ and sulfate emissions decrease. Even so, because G6Sulfur involves injecting sulfate directly into the stratosphere, sulfate deposition stays remarkably constant from 2015 to 2100. The fact that it does not increase rapidly or in sharp increments means that much of the injected sulfate is staying in the atmosphere to reduce radiative forcing, as intended. However, not all of it is, meaning these injections will have to continue throughout the whole time period to maintain the same level of radiative forcing impact.

The difference in location between emissions and deposition in future scenarios (Fig. 3, S4) highlights the role of long-range transport in distributing sulfur from source to sink (Fisher, 1975). Much of the projected decline in both deposition and emissions is happening between the 2020–2040 time period and the 2041–2060 period. While the drop in emissions is quick, the impacts are spread between multiple ecoregions such that, with the exception of mixed forest and open shrublands, most ecoregions experience a steady decrease throughout the century. However, it is not yet known whether even this relatively slow change is tolerable by the species that are either suddenly now not receiving enough sulfur or, in the case of mixed forest and open shrubland, experience a sharp decline and then a sharp and almost equal increase within the span of 40 years. If SAI were terminated early and unexpectedly, the sulfur deposition would adjust within a year or two to the levels projected by the relevant SSP, commensurate with the level of $CO_2$ in the atmosphere. In some cases, this could be catastrophic.

While modeling with CMIP5 ensembles suggests reductions in precipitation in many regions from an SAI scenario (Cheng et al., 2019; Simpson et al., 2019), recent work with CMIP6 models points out that the precipitation effects will strongly depend on the strategy and magnitude of the climate intervention (Tilmes et al., 2020); our results show an overall slight increase in precipitation (Figure S2). This suggests that the cooling effect of SAI is not enough to entirely restore pre-industrial precipitation regimes in all regions as local climate variability may mask the impact of SAI (Irvine et al., 2019; Irvine and Keith, 2020; Tye et al., 2022). The new patterns of precipitation in many regions may also impact nitrogen deposition and therefore carbon sequestration and nutrient availability for croplands. As of yet, no G6 Sulfur models include enough variables to determine if this is the case.

It should be noted that currently nitrogen is not included in the GeoMIP models so the effects of SAI on deposition do not include any interaction with the nitrogen cycle. Models would more closely capture reality if they were to include nitrogen deposition, particularly in regions that are known to have high emissions that will likely continue to increase (Sun et al., 2022). There is also no sulfur transport from fires.

Past work has shown that it is feasible to replicate injection strategies between models producing similar temperature responses (Visioni et al., 2023). Coordinating such efforts to include a thought-out strategy for temperature targets and injection latitudes would greatly help with comparability between future scenarios and a better understanding of the risks and benefits of SAI.

## 7. Conclusions

Although controversial, SAI is a technologically feasible method of buying time for the world to slow down climate change. As such, it is important to evaluate the climate risks and human and environmental impacts of enacting this strategy globally. This work evaluates sulfur deposition under G6sulfur and compares the projections with SSP2-4.5 and SSP5-8.5 scenarios. Our results demonstrate that the injections required to maintain G6 Sulfur conditions and mitigate warming will have non-negligible impacts on sensitive ecoregions when compared to both SSP2-4.5 and SSP5-8.5. While dry deposition will continue to decline under all 3 future scenarios, the ratio of wet to dry deposition will change under G6 Sulfur, especially on a seasonal basis as more wet deposition occurs even in historically drier seasons. And, importantly, the benefits from SAI in terms of lower sulfur deposition to sensitve ecoregions are concentrated in the near future. We also point out that there are large discrepancies across models and injection strategies, meaning that deposition will depend on which strategy is chosen as well as the stratospheric dynamics and chemical processes that differ between models. This area of uncertainty contains a broad range of outcomes that are hard to sample, especially when including other interactions such as nitrogen-sulfur interactions, fire inputs, and stratosphere-troposphere interactions.

## Declaration of Competing Interest

The authors declare that they have no known competing financial interests or personal relationships that could have appeared to influence the work reported in this paper.

## Data availability

Data will be made available on request.

## Acknowledgements

This research used resources of the Oak Ridge Leadership Computing Facility (OLCF) at Oak Ridge National Laboratory (ORNL), which is managed by UT-Battelle, LLC, for the US Department of Energy under Contract No. DE-AC05-00OR22725.

## Appendix A. Supporting information

Supplementary data associated with this article can be found in the online version at doi:10.1016/j.gecadv.2024.100011.

## References


Aas, W., Mortier, A., Bowersox, V., Cherian, R., Faluvegi, G., Fagerli, H., Hand, J., Klimont, Z., Galy-Lacaux, C., Lehmann, C.M.B., Myhre, C.L., Myhre, G., Olivié, D., Sato, K., Quaas, J., Rao, P.S.P., Schulz, M., Shindell, D., Skeie, R.B., Stein, A., Takemura, T., Tsyro, S., Vet, R., Xu, X., 2019. Global and regional trends of atmospheric sulfur. Sci. Rep 9, 953. https://doi.org/10.1038/s41598-018-37304-0.

Cheng, I., Zhang, L., He, Z., Cathcart, H., Houle, D., Cole, A., Feng, J., O'Brien, J., Macdonald, A.M., Aherne, J., Brook, J., 2022. Long-term declines in atmospheric nitrogen and sulfur deposition reduce critical loads exceedances at multiple Canadian rural sites, 2000–2018. Atmosp.Chem. Phys. 22, 14631–14656. https://doi.org/10.5194/acp-22-14631-2022.

Cheng, W., MacMartin, D.G., Dagon, K., Kravitz, B., Tilmes, S., Richter, J.H., Mills, M.J., Simpson, I.R., 2019. Soil Moisture and Other Hydrological Changes in a Stratospheric Aerosol Geoengineering Large Ensemble. J. Geophys. Res. Atmosp. 124, 12773–12793. https://doi.org/10.1029/2018JD030237.

Clark, B., Xia, L., Robock, A., Tilmes, S., Richter, J.H., Visioni, D., Rabin, S.S., 2023. Optimal climate intervention scenarios for crop production vary by nation. Nat Food 4, 902–911. https://doi.org/10.1038/s43016-023-00853-3.

Crutzen, P.J., 2006. Albedo Enhancement by Stratospheric Sulfur Injections: a Contribution to Resolve a Policy Dilemma? Clim. Change 77, 211–220. https://doi.org/10.1007/s10584-006-9101-y.

d'Arge, R.C., Schulze, W.D., Brookshire, D.S., 1982. Carbon dioxide and intergenerational choice. Am. Econ. Rev. 72, 251–256.

Doney, S.C., Mahowald, N., Lima, I., Feely, R.A., Mackenzie, F.T., Lamarque, J.-F., Rasch, P.J., 2007. Impact of anthropogenic atmospheric nitrogen and sulfur deposition on ocean acidification and the inorganic carbon system. PNAS 104, 14580–14585. https://doi.org/10.1073/pnas.0702218104.

Driscoll, C.T., Lawrence, G.B., Bulger, A.J., Butler, T.J., Cronan, C.S., Eagar, C., Lambert, K.F., Likens, G.E., Stoddard, J.L., Weathers, K.C., 2001. Acidic Deposition in the Northeastern United States: Sources and Inputs, Ecosystem Effects, and Management Strategies: The effects of acidic deposition in the northeastern United States include the acidification of soil and water, which stresses terrestrial and aquatic biota. BioScience 51, 180–198 https://doi.org/10.1641/0006-3568(2001)051[0180:ADITNU]2.0.CO;2.

Eastham, S.D., Weisenstein, D.K., Keith, D.W., Barrett, S.R.H., 2018. Quantifying the impact of sulfate geoengineering on mortality from air quality and UV-B exposure. Atmos. Environ. 187, 424–434. https://doi.org/10.1016/j.atmosenv.2018.05.047.

Eyring, V., Bony, S., Meehl, G.A., Senior, C.A., Stevens, B., Stouffer, R.J., Taylor, K.E., 2016. Overview of the Coupled Model Intercomparison Project Phase 6 (CMIP6) experimental design and organization. Geosci. Model Dev. 9, 1937–1958. https://doi.org/10.5194/gmd-9-1937-2016.

Fisher, B.E.A., 1975. The long range transport of sulphur dioxide. Atmos. Environ. 9, 1063–1070. https://doi.org/10.1016/0004-6981(75)90180-8.

Galloway, J.N., 1995. Acid deposition: Perspectives in time and space. Water Air Soil Pollut. 85, 15–24. https://doi.org/10.1007/BF00483685.

Ge, X., Yu, Q., Duan, L., Zhao, Y., Posch, M., Hao, J., 2023. High-resolution maps of critical loads for sulfur and nitrogen in China. Sci. Data 10, 339. https://doi.org/10.1038/s41597-023-02178-z.

Geiser, L.H., Root, H., Smith, R.J., Jovan, S.E., St Clair, L., Dillman, K.L., 2021. Lichen-based critical loads for deposition of nitrogen and sulfur in US forests. Environ. Pollut. 291, 118187 https://doi.org/10.1016/j.envpol.2021.118187.

Grasso, M., 2019. Sulfur in the Sky with Diamonds: An Inquiry into the Feasibility of Solar Geoengineering. Global Policy 10, 217–226. https://doi.org/10.1111/1758-5899.12646.

Gu, L., Baldocchi, D.D., Wofsy, S.C., Munger, J.W., Michalsky, J.J., Urbanski, S.P., Boden, T.A., 2003. Response of a Deciduous Forest to the Mount Pinatubo Eruption: Enhanced Photosynthesis. Science 299, 2035–2038. https://doi.org/10.1126/science.1078366.

Hargrove, W.W., Hoffman, F.M., 2004. Potential of Multivariate Quantitative Methods for Delineation and Visualization of Ecoregions. Environ. Manag. 34, S39–S60. https://doi.org/10.1007/s00267-003-1084-0.

Hargrove, W.W., Hoffman, F.M., Hessburg, P.F., 2006. Mapcurves: a quantitative method for comparing categorical maps. J. Geograph. Syst. 8, 187. https://doi.org/10.1007/s10109-006-0025-x.

Hepburn, C., Adlen, E., Beddington, J., Carter, E.A., Fuss, S., Mac Dowell, N., Minx, J.C., Smith, P., Williams, C.K., 2019. The technological and economic prospects for CO2 utilization and removal. Nature 575, 87–97. https://doi.org/10.1038/s41586-019-1681-6.

IPCC, 2022. Climate Change 2022: Impacts, Adaptation and Vulnerability (Scientific Investigations Report), Contributions of Working Group II teo the Sixth Assessment Report of the Intergovernemental Panel on Climate Change. IPCC, Cambridge University Press.

Irvine, P., Emanuel, K., He, J., Horowitz, L.W., Vecchi, G., Keith, D., 2019. Halving warming with idealized solar geoengineering moderates key climate hazards. Nat. Clim. Chang. 9, 295–299. https://doi.org/10.1038/s41558-019-0398-8.

Irvine, P.J., Keith, D.W., 2020. Halving warming with stratospheric aerosol geoengineering moderates policy-relevant climate hazards. Environ. Res. Lett. 15, 044011 https://doi.org/10.1088/1748-9326/ab76de.

Kortetmäki, T., Oksanen, M., 2023. Right to Food and Geoengineering. J. Agric. Environ. Ethics 36, 5. https://doi.org/10.1007/s10806-023-09898-7.

Kravitz, B., Robock, A., Boucher, O., Schmidt, H., Taylor, K.E., Stenchikov, G., Schulz, M., 2011. The Geoengineering Model Intercomparison Project (GeoMIP). Atmos. Sci. Lett. 12, 162–167. https://doi.org/10.1002/asl.316.

Kravitz, B., Robock, A., Tilmes, S., Boucher, O., English, J.M., Irvine, P.J., Jones, A., Lawrence, M.G., MacCracken, M., Muri, H., Moore, J.C., Niemeier, U., Phipps, S.J., Sillmann, J., Storelvmo, T., Wang, H., Watanabe, S., 2015. The Geoengineering Model Intercomparison Project Phase 6 (GeoMIP6): simulation design and preliminary results. Geosci. Model Dev. 8, 3379–3392. https://doi.org/10.5194/gmd-8-3379-2015.

Lamarque, J.-F., Dentener, F., McConnell, J., Ro, C.-U., Shaw, M., Vet, R., Bergmann, D., Cameron-Smith, P., Dalsoren, S., Doherty, R., Faluvegi, G., Ghan, S.J., Josse, B., Lee, Y.H., MacKenzie, I.A., Plummer, D., Shindell, D.T., Skeie, R.B., Stevenson, D.S., Strode, S., Zeng, G., Curran, M., Dahl-Jensen, D., Das, S., Fritzsche, D., Nolan, M., 2013. Multi-model mean nitrogen and sulfur deposition from the Atmospheric Chemistry and Climate Model Intercomparison Project (ACCMIP): evaluation of historical and projected future changes. Atmosp. Chem. 13, 7997–8018. https://doi.org/10.5194/acp-13-7997-2013.

Lanning, M., Wang, L., Scanlon, T.M., Vadeboncoeur, M.A., Adams, M.B., Epstein, H.E., Druckenbrod, D., 2019. Intensified vegetation water use under acid deposition. Sci. Adv. 5, eaav5168 https://doi.org/10.1126/sciadv.aav5168.

Lawrence, M.G., Schäfer, S., Muri, H., Scott, V., Oschlies, A., Vaughan, N.E., Boucher, O., Schmidt, H., Haywood, J., Scheffran, J., 2018. Evaluating climate geoengineering proposals in the context of the Paris Agreement temperature goals. Nat. Commun. 9, 3734. https://doi.org/10.1038/s41467-018-05938-3.

Lee, W., MacMartin, D., Visioni, D., Kravitz, B., 2020. Expanding the Design Space of Stratospheric Aerosol Geoengineering to Include Precipitation-Based Objectives and Explore Trade-offs (preprint). Management of the Earth system: engineering responses to climate change. ⟨https://doi.org/10.5194/esd-2020-58⟩.

Long, J.C.S., Shepherd, J.G., 2014. The Strategic Value of Geoengineering Research. In: Freedman, B. (Ed.), Global Environmental Change, Handbook of Global Environmental Pollution. Springer Netherlands, Dordrecht, pp. 757–770. https://doi.org/10.1007/978-94-007-5784-4_24.

McMurray, J.A., McDonnell, T.C., Mebane, A., Pardo, L., 2021. Assessment of Atmospheric Nitrogen and Sulfur Deposition Critical Loads for Aquatic and Terrestrial Resources on National Forest System Lands in the Intermountain Region (Technical Report No. NRS-204). Madison, WI: U.S. Department of Agriculture, Forest Service, Northern Research Station.

National Research Council, 2015. Climate Intervention: Reflecting Sunlight to Cool Earth. https://doi.org/10.17226/18988.

Neary, B.P., Dillon, P.J., 1988. Effects of sulphur deposition on lake-water chemistry in Ontario, Canada. Nature 333, 340–343. https://doi.org/10.1038/333340a0.

Niemeier, U., Timmreck, C., 2015. What is the limit of climate engineering by stratospheric injection of $SO_2$? Atmos. Chem. Phys. 15, 9129–9141. https://doi.org/10.5194/acp-15-9129-2015.

Nilsson, J., 1988. Critical Loads for Sulphur and Nitrogen. In: Mathy, P. (Ed.), Air Pollution and Ecosystems. Springer Netherlands, Dordrecht, pp. 85–91. https://doi.org/10.1007/978-94-009-4003-1_11.

O'Neill, B.C., Tebaldi, C., van Vuuren, D.P., Eyring, V., Friedlingstein, P., Hurtt, G., Knutti, R., Kriegler, E., Lamarque, J.-F., Lowe, J., Meehl, G.A., Moss, R., Riahi, K., Sanderson, B.M., 2016. The Scenario Model Intercomparison Project (ScenarioMIP) for CMIP6. Geosci. Model Dev. 9, 3461–3482. https://doi.org/10.5194/gmd-9-3461-2016.

Pavlovic, N.R., Chang, S.Y., Huang, J., Craig, K., Clark, C., Horn, K., Driscoll, C.T., 2023. Empirical nitrogen and sulfur critical loads of U.S. tree species and their uncertainties with machine learning. Sci. Total Environ. 857, 159252 https://doi.org/10.1016/j.scitotenv.2022.159252.

Pye, H.O.T., Nenes, A., Alexander, B., Ault, A.P., Barth, M.C., Clegg, S.L., Collett Jr, J.L., Fahey, K.M., Hennigan, C.J., Herrmann, H., Kanakidou, M., Kelly, J.T., Ku, I.-T., McNeill, V.F., Riemer, N., Schaefer, T., Shi, G., Tilgner, A., Walker, J.T., Wang, T., Weber, R., Xing, J., Zaveri, R.A., Zuend, A., 2020. The acidity of atmospheric particles and clouds. Atmos. Chem. 20, 4809–4888. https://doi.org/10.5194/acp-20-4809-2020.

R Core Team, 2022. R: A Language and Environment for Statistical Computing.

Riahi, K., van Vuuren, D.P., Kriegler, E., Edmonds, J., O'Neill, B.C., Fujimori, S., Bauer, N., Calvin, K., Dellink, R., Fricko, O., Lutz, W., Popp, A., Cuaresma, J.C., Kc, S., Leimbach, M., Jiang, L., Kram, T., Rao, S., Emmerling, J., Ebi, K., Hasegawa, T., Havlik, P., Humpenöder, F., Da Silva, L.A., Smith, S., Stehfest, E., Bosetti, V., Eom, J., Gernaat, D., Masui, T., Rogelj, J., Strefler, J., Drouet, L., Krey, V., Luderer, G., Harmsen, M., Takahashi, K., Baumstark, L., Doelman, J.C., Kainuma, M., Klimont, Z., Marangoni, G., Lotze-Campen, H., Obersteiner, M., Tabeau, A., Tavoni, M., 2017. The Shared Socioeconomic Pathways and their energy, land use, and greenhouse gas emissions implications: An overview. Glob. Environ. Change 42, 153–168. https://doi.org/10.1016/j.gloenvcha.2016.05.009.

Robiou du Pont, Y., Meinshausen, M., 2018. Warming assessment of the bottom-up Paris Agreement emissions pledges. Nat. Commun. 9, 4810. https://doi.org/10.1038/s41467-018-07223-9.

Rubin, H.J., Fu, J.S., Dentener, F., Li, R., Huang, K., Fu, H., 2023. Global nitrogen and sulfur deposition mapping using a measurement–model fusion approach. Atmos. Chem. Phys. 23, 7091–7102. https://doi.org/10.5194/acp-23-7091-2023.

Scheffers, B.R., De Meester, L., Bridge, T.C.L., Hoffmann, A.A., Pandolfi, J.M., Corlett, R. T., Butchart, S.H.M., Pearce-Kelly, P., Kovacs, K.M., Dudgeon, D., Pacifici, M., Rondinini, C., Foden, W.B., Martin, T.G., Mora, C., Bickford, D., Watson, J.E.M., 2016. The broad footprint of climate change from genes to biomes to people. Science 354, aaf7671. https://doi.org/10.1126/science.aaf7671.

Schultz, P.A., Kasting, J.F., 1997. Optimal reductions in CO2 emissions. Energy Policy 25, 491–500. https://doi.org/10.1016/S0301-4215(97)00027-X.

Schulzweida, U., 2021. CDO User Guide. ⟨https://doi.org/10.5281/zenodo.5614769⟩.

Séférian, R., Nabat, P., Michou, M., Saint-Martin, D., Voldoire, A., Colin, J., Decharme, B., Delire, C., Berthet, S., Chevallier, M., Sénési, S., Franchisteguy, L., Vial, J., Mallet, M., Joetzjer, E., Geoffroy, O., Guérémy, J.-F., Moine, M.-P., Msadek, R., Ribes, A., Rocher, M., Roehrig, R., Salas-y-Mélia, D., Sanchez, E.,

Terray, L., Valcke, S., Waldman, R., Aumont, O., Bopp, L., Deshayes, J., Éthé, C., Madec, G., 2019. Evaluation of CNRM Earth System Model, CNRM-ESM2-1: Role of Earth System Processes in Present-Day and Future Climate. Journal of Advances in Modeling Earth Systems 11, 4182–4227. https://doi.org/10.1029/2019MS001791.

Shao, S., Driscoll, C.T., Sullivan, T.J., Burns, D.A., Baldigo, BarryP., Lawrence, G.B., McDonnell, T.C., 2020. The response of stream ecosystems in the Adirondack region of New York to historical and future changes in atmospheric deposition of sulfur and nitrogen. Science of The Total Environment 716, 137113. https://doi.org/10.1016/j.scitotenv.2020.137113.

Shepherd, J.G., 2012. Geoengineering the climate: an overview and update. Philosophical Transactions of the Royal Society A: Mathematical, Physical and Engineering Sciences 370, 4166–4175. https://doi.org/10.1098/rsta.2012.0186.

Simpson, I.R., Tilmes, S., Richter, J.H., Kravitz, B., MacMartin, D.G., Mills, M.J., Fasullo, J.T., Pendergrass, A.G., 2019. The Regional Hydroclimate Response to Stratospheric Sulfate Geoengineering and the Role of Stratospheric Heating. J. Geophy. Res. Atmos. 124, 12587–12616. https://doi.org/10.1029/2019JD031093.

Smith, S.J., Andres, R., Conception, E., Lurz, J., 2004. Historical Sulfur Dioxide Emissions 1850-2000: Methods and Results (No. PNNL-14537, 15020102). ⟨https://doi.org/10.2172/15020102⟩.

Smith, W., Henly, C., 2021. Updated and outdated reservations about research into stratospheric aerosol injection. Clim. Change 164, 39. https://doi.org/10.1007/s10584-021-03017-z.

Smith, W., Wagner, G., 2018. Stratospheric aerosol injection tactics and costs in the first 15 years of deployment. Environ. Res. Lett. 13, 124001 https://doi.org/10.1088/1748-9326/aae98d.

Sun, K., Gao, Y., Guo, X., Zhang, J., Zeng, X., Ma, M., Chen, Y., Luo, K., Yao, X., Gao, H., 2022. The enhanced role of atmospheric reduced nitrogen deposition in future over East Asia–Northwest Pacific. Sci. Total Environ. 833, 155146 https://doi.org/10.1016/j.scitotenv.2022.155146.

Tilmes, S., MacMartin, D.G., Lenaerts, J.T.M., van Kampenhout, L., Muntjewerf, L., Xia, L., Harrison, C.S., Krumhardt, K.M., Mills, M.J., Kravitz, B., Robock, A., 2020. Reaching 1.5 and 2.0 °C global surface temperature targets using stratospheric aerosol geoengineering. Earth Syst. Dyn. 11, 579–601. https://doi.org/10.5194/esd-11-579-2020.

Tilmes, S., Mills, M.J., Niemeier, U., Schmidt, H., Robock, A., Kravitz, B., Lamarque, J.-F., Pitari, G., English, J.M., 2015. A new Geoengineering Model Intercomparison Project (GeoMIP) experiment designed for climate and chemistry models. Geoscientific Model Development 8, 43–49. https://doi.org/10.5194/gmd-8-43-2015.

Tilmes, S., Visioni, D., Jones, A., Haywood, J., Séférian, R., Nabat, P., Boucher, O., Bednarz, E.M., Niemeier, U., 2022. Stratospheric ozone response to sulfate aerosol and solar dimming climate interventions based on the G6 Geoengineering Model Intercomparison Project (GeoMIP) simulations. Atmos. Chem. Phys. 22, 4557–4579. https://doi.org/10.5194/acp-22-4557-2022.

Tjiputra, J.F., Grini, A., Lee, H., 2016. Impact of idealized future stratospheric aerosol injection on the large-scale ocean and land carbon cycles. J.Geophy. Res. Biogeosci. 121, 2–27. https://doi.org/10.1002/2015JG003045.

Tollefson, 2019. The hard truths of climate change — by the numbers. Nature 573, 324.

Townshend, J.R.G., 1992. Improved global data for land applications. A proposal for a new high resolution data set. Report of the Land Cover Working Group of IGBP-DIS. Global Change Report (Sweden).

Tracy, S.M., Moch, J.M., Eastham, S.D., Buonocore, J.J., 2022. Stratospheric aerosol injection may impact global systems and human health outcomes. Elem.: Sci. Anthrop. 10, 00047 https://doi.org/10.1525/elementa.2022.00047.

Tye, M.R., Dagon, K., Molina, M.J., Richter, J.H., Visioni, D., Kravitz, B., Tilmes, S., 2022. Indices of extremes: geographic patterns of change in extremes and associated vegetation impacts under climate intervention. Earth Syst. Dyn. 13, 1233–1257. https://doi.org/10.5194/esd-13-1233-2022.

Visioni, D., Pitari, G., Tuccella, P., Curci, G., 2017. Quantification of sulfur deposition changes under sulfate geoengineering conditions (preprint). Aerosols/Atmospheric Modelling/Stratosphere/Physics (physical properties and processes). ⟨https://doi.org/10.5194/acp-2017-987⟩.

Visioni, D., Pitari, G., Tuccella, P., Curci, G., 2018. Sulfur deposition changes under sulfate geoengineering conditions: quasi-biennial oscillation effects on the transport and lifetime of stratospheric aerosols. Atmos. Chem. 18, 2787–2808. https://doi.org/10.5194/acp-18-2787-2018.

Visioni, D., Slessarev, E., MacMartin, D.G., Mahowald, N.M., Goodale, C.L., Xia, L., 2020. What goes up must come down: impacts of deposition in a sulfate geoengineering scenario. Environ. Res. Lett. 15, 094063 https://doi.org/10.1088/1748-9326/ab94eb.

Visioni, D., MacMartin, D.G., Kravitz, B., Boucher, O., Jones, A., Lurton, T., Martine, M., Mills, M.J., Nabat, P., Niemeier, U., Séférian, R., Tilmes, S., 2021. Identifying the sources of uncertainty in climate model simulations of solar radiation modification with the G6sulfur and G6solar Geoengineering Model Intercomparison Project (GeoMIP) simulations. Atmos. Chem. Phys. 21, 10039–10063. https://doi.org/10.5194/acp-21-10039-2021.

Visioni, D., Bednarz, E.M., Lee, W.R., Kravitz, B., Jones, A., Haywood, J.M., MacMartin, D.G., 2023. Climate response to off-equatorial stratospheric sulfur injections in three Earth system models – Part 1: Experimental protocols and surface changes. Atmos. Chem. Phys. 23, 663–685. https://doi.org/10.5194/acp-23-663-2023.

Wu, D., Zhao, X., Liang, S., Zhou, T., Huang, K., Tang, B., Zhao, W., 2015. Time-lag effects of global vegetation responses to climate change. Glob. Change Biol. 21, 3520–3531. https://doi.org/10.1111/gcb.12945.

Xu, Y., Lin, L., Tilmes, S., Dagon, K., Xia, L., Diao, C., Cheng, W., Wang, Z., Simpson, I., Burnell, L., 2020. Climate engineering to mitigate the projected 21st-century terrestrial drying of the Americas: a direct comparison of carbon capture and sulfur injection. Earth System Dyn. 11, 673–695. https://doi.org/10.5194/esd-11-673-2020.

Yang, C.-E., Hoffman, F.M., Ricciuto, D.M., Tilmes, S., Xia, L., MacMartin, D.G., Kravitz, B., Richter, J.H., Mills, M., Fu, J.S., 2020. Assessing terrestrial biogeochemical feedbacks in a strategically geoengineered climate. Environ. Res. Lett. 15, 104043 https://doi.org/10.1088/1748-9326/abacf7.

Zhou, K., Zhao, Y., Zhang, L., Xi, M., 2021. Declining dry deposition of NO2 and SO2 with diverse spatiotemporal patterns in China from 2013 to 2018. Atmos. Environ. 262, 118655 https://doi.org/10.1016/j.atmosenv.2021.118655.